System Identification of a Wind Turbine Array

Jennifer Annoni*, Kevin Howard†, Peter Seiler‡, and Michele Guala§
Department of Aerospace Engineering & Mechanics
University of Minnesota, Minneapolis, MN, 55455, USA

Individual wind turbines, whether stand alone or in a wind farms, typically operate to maximize their own production without considering the impact of wake effects on nearby turbines. Investigation into wind turbine interaction within a wind farm has the potential to increase total power and reduce structural loads by properly coordinating the individual turbines that comprise the wind farm. To effectively design and analyze such coordinated controllers requires turbine wake models of sufficient accuracy. This paper develops a dynamic model, derived from experiments, to describe the aerodynamic interactions between two model turbines in a wind tunnel. Experiments were conducted in the atmospheric boundary layer wind tunnel at the Saint Anthony Falls Laboratory at the University of Minnesota and were performed by varying the voltage input to the upwind turbine. Particle Image Velocimetry (PIV) and voltage measurements were used to capture the physical evolution of the interactions of the turbines as well as measure the response of the turbines, respectively. A transfer function model relating the upwind turbine input to downwind turbine output was identified from the experimental data. Following a few modifications to the current setup, future work will include performing wind farm control using the dynamic model presented in this paper.

Nomenclature

A	Rotor Area, $[m^2]$
β	pitch angle, $[rad]$
C_p	Power coefficient, []
P	Power captured by the turbine, $[W]$
ρ	air density, $[kg/m^3]$
u	wind speed, $[m/s]$
R	Rotor radius, $[m]$
λ	tip-speed ratio, []
ω	rotor speed, [rad/s]
J	rotational inertia, [kg/m^2]
τ_{aero}	aerodynamic torque, [Nm]
τ_g	generator torque, [Nm]

I. Introduction

Many state governments in the U.S. have set renewable portfolio standards that mandate renewable energy targets. For example, Minnesota has a target of 25% renewable energy by 2025.[1] Wind energy is a fast growing source of renewable energy, hence it is a key component to meet these standards. Achieving these targets requires increasing the efficiency and reducing the overall costs of wind energy. In particular, increasing the production efficiency of existing wind farms is critical as suitable land for turbines is decreasing.

*Graduate Student, Department of Aerospace Engineering and Mechanics, anno0010@umn.edu
†Graduate Student, Saint Anthony Falls Laboratory
‡Assistant Professor, Department of Aerospace Engineering and Mechanics
§Assistant Professor, Department of Civil Engineering

In addition, reducing structural loads on turbines will improve the economic competitiveness of wind energy by reducing the operation and maintenance costs and increasing the lifetime of the turbines.

Currently, wind turbines are usually controlled individually to maximize their own performance. Many studies have shown that operating all turbines in a wind farm at their optimal operating point leads to suboptimal performance of the overall wind farm.[2–8] An improved understanding of the aerodynamic interactions between turbines can aid in the design of enhanced control strategies that coordinate all turbines in a farm. The papers cited above present coordinated turbine control strategies with the aim of increasing the total wind farm power and, in some cases, reducing the structural loads. The essential idea is that derating the lead turbine results in higher wind speeds for downwind turbines. Proper derating can result in a higher total power than simply operating each turbine at its own peak efficiency.

Most of the prior work on coordinated turbine control has used simplified actuator disk models for the design and analysis.[9–15] More accurate wake modeling is necessary to help understand and quantify the aerodynamic interactions in a wind farm. A variety of wake models exist in literature that are useful for studying wind farm control. The simplest, quasi-static models are the Park model[9] and the eddy viscosity model.[10] These models provide a quick, preliminary description of the wake interactions in a wind farm, but neglect some key dynamics. There are also several high fidelity computational fluid dynamics (CFD) models that have been developed.[16,17] These high-fidelity models are the most accurate tools and can be used for evaluating wind farm controllers. However, they are computationally expensive. Control design requires simplified dynamical models that capture the essential dynamics.

This paper develops a turbine model suitable for wind farm control using experimental results and system identification techniques. These experiments are performed in a wind tunnel using two model turbines. Traditional wind turbine and wind tunnel experiments have been done looking at different characteristics such as topographical effects and upwind previewing.[18,19] In addition, some studies have been done looking at the performance of a two turbine array and the impact of the upwind turbine on the downwind turbine.[20–26] The experiments presented in this paper build upon the existing literature with the goal of formulating a model describing the interactions between two turbines suitable for wind farm control. This has been done by varying the input to the upwind turbine and observing the effects on the downwind turbine. Voltage measurements and PIV are used to gain insight into the aerodynamics interactions within the two turbine array. The wind tunnel data collected from these experiments also provides some insight as to the time and spatial scales of interest in wind farm control. Lastly, the data-driven method proposed in this paper could be used to construct dynamic turbine coupling models from field data.

The remainder of this paper proceeds as follows: section II gives a brief description of single turbine control, specifically targeting the control parameters used in the experiments, section III provides details of the experimental setup of the two-turbine array in the wind tunnel. Results from these experiments are presented in Section IV followed by the system identification techniques used to generate a model for the two-turbine setup in Section V. Finally, conclusions and suggestions for future work are given in Section VI.

II. Wind Turbine Dynamics and Control Design

This section briefly reviews the operation and control of a single turbine. Additional details and references can be found in.[27–29] Utility-scale turbines have several inputs that can be controlled to increase the power production and reduce structural loads. These inputs include generator torque, τ_g, and the blade pitch angle, β, which can control the rotor speed of the turbine, ω for a given wind speed u. In general, the generator torque is varied at low wind speeds to maximize power captured. At high wind speeds, the blade pitch angle is used to mitigate mechanical and electrical loads. The power captured by a single turbine can be expressed by:

$$P = \frac{1}{2}\rho A U^3 C_P(\beta, \lambda) \tag{1}$$

where ρ [kg/m^3] is the air density, A, [m^2] is the area swept by the rotor, u [m/s] is the wind speed perpendicular to the rotor plane, and C_P is the power coefficient. The C_P is the fraction of available power in the wind captured by the wind turbine, or efficiency of the turbine, and is a function of blade pitch angle, β [rad] and the nondimensional tip-speed ratio. Figure 1 is the normalized C_P curve of the 2.5 MW Clipper turbine located at the University of Minnesota's Eolos wind research station in UMore Park, Rosemount, MN. The peak efficiency has been normalized for proprietary reasons. Tip-speed ratio is defined as $\lambda = \frac{\omega R}{u}$,

where ω [rad/s] is the rotor speed and R [m] is the rotor radius. The peak C_{P_*} value is achieved at some fixed blade pitch angle, β_*, while tip-speed ratio changes with varying wind speed. The optimal tip-speed ratio, λ_*, can be achieved by changing the rotor speed proportionally to the wind variations. The standard turbine controller, with torque and blade pitch as inputs, can be split into 3 regions (see Figure 2): Region 1, Region 2, and Region 3. In Region 1, the turbine does not produce any power because the wind speed is not sufficient to operate. Once the wind reaches the cut-in speed, the turbine enters Region 2. In this region, the turbine keeps the blades fixed at an optimal blade pitch angle and maximizes the generator torque to maximize the power of the turbine. Lastly, when the wind reaches the rated wind speed, the turbine is producing the maximum power that it is allowed to produce. In this region, the power is held constant by fixing the generator torque. As wind speed increases, the blades are pitched to minimize structural loads and maintain a constant rotor speed. The specifics of the controller operation in each region are addressed below.

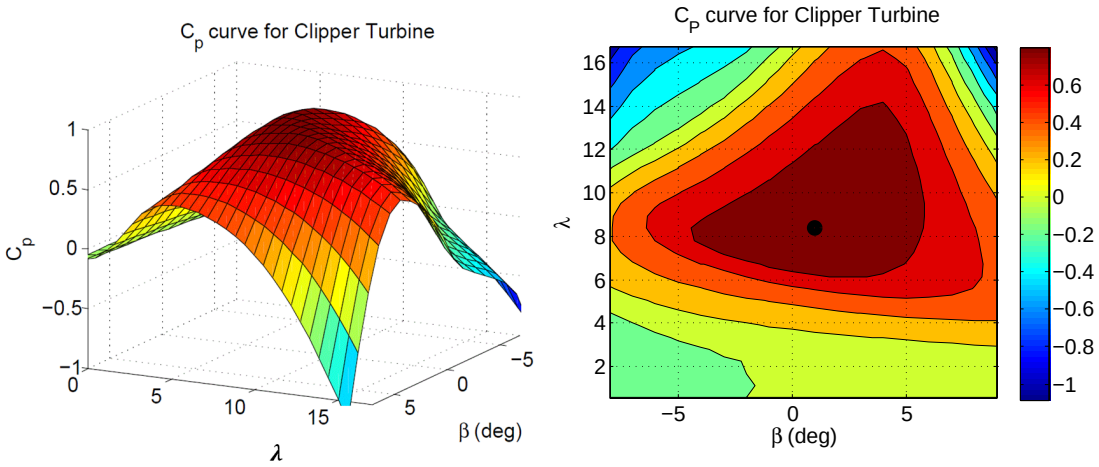

Figure 1. C_p **curve of the 2.5MW Clipper turbine at UMore Park, Minnesota**

In Region 2, the controller typically used is a generator torque controller. The dynamics of the turbine are modeled as a single degree-of-freedom rotational system:

$$\dot{\omega} = \frac{1}{J}\left(\tau_{aero} - \tau_g\right) \tag{2}$$

where $\dot{\omega}$ [rad/s^2] is the angular acceleration, τ_{aero} [Nm] is the aerodynamic torque, and τ_g [Nm] is the generator torque. The power captured by a turbine can be expressed in terms of rotor speed:

$$P = \tau_{aero}\omega \tag{3}$$

Using this relationship, the aerodynamic torque can be rewritten as:

$$\tau_{aero} = \frac{P}{\omega} = \frac{\rho A u^3 C_P(\beta, \lambda)}{2\omega} \tag{4}$$

The objective of a generator torque controller is to maximize power. This is done by maintaining an optimal blade pitch angle, β_*, and tip-speed ratio, λ_*. The blade pitch angle is held fixed at β_*, and the generator torque is controlled to achieve λ_* in varying wind conditions. The generator torque can be computed using the standard control law:

$$\tau_g = K_g\omega^2 \tag{5}$$

where $K_g = \frac{C_{P_*}\rho A R^5}{2\lambda_*^3}$ and N is the gearbox ratio. If K_g is chosen properly, the power from the turbine will converge to C_{P_*} in steady winds. In turbulent winds, the turbine will cycle around the peak λ_*. Substituting τ_{aero} and τ_g into a single degree-of-freedom rotational system, it can be shown that the turbine will converge

toward the desired operating point $C_{P_*}(\beta_*, \lambda_*)$. The experiments described in later sections focus on turbine operation in Region 2 where the generator torque is used to control the turbines.

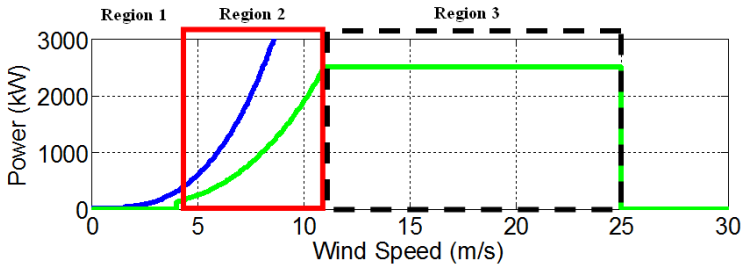

Figure 2. Regions of wind turbine operation

In Region 3, the turbine controller holds the generator torque constant and pitches the blades to minimize structural loads. It is common to use a PI or PID controller for blade pitch control [17], [18]. This region is not addressed in experiments and may be looked at in future experiments.

III. Experimental Setup

A. Wind Tunnel

The experiments were completed in a closed loop wind tunnel at SAFL on the campus of the University of Minnesota. A 200 horse-power fan drives the flow in the tunnel, into the test section which has a length of 16 m and a cross-section of 1.7 m by 1.7 m. Coarse wire mesh and a honeycomb flow straightener condition the flow prior to entering a contraction with an area ratio of 6.6:1 upwind of the main test section. Immediately at the end of the contraction, a trip is placed to promote boundary layer growth.

The scale turbines were placed roughly 13 m downwind of the trip in the test section where a turbulent boundary layer thickness of $\delta \approx 0.6$ m was measured for the neutral boundary layer. The logarithmic velocity profile has a well-developed surface layer and the ceiling is adjusted to ensure a zero pressure gradient within the test section. The surface (floor of the tunnel) is composed of smooth, aluminum plates, each with a length of 0.3 m in the flow direction and can be heated or cooled to produce the desired thermal boundary layer. In addition to the floor temperature control, the air temperature is maintained by a large radiator located downwind of the tunnel fan. The neutral cases investigated herein set the air and floor temperature equal, and were held to within $\pm 0.2°$C.

The wind turbine models tested in the tunnel are approximately 1:750 scale models of the Clipper Liberty 2.5MW utility-scale wind turbine, see Figure 3. The resulting dimensions for the model are a three-blade rotor with a diameter of 0.128 m (GWS/EP-5030x3 rotor designed for model aircraft). The blades are oriented such that high pressure surface faces the inflow. The hub height is 0.104 m and remains within the lower twenty-five percent of the boundary layer, similar to the full-scale turbine from which it was scaled. The tip-speed ratio, λ, was controlled by carefully selecting the model turbine generator and is on the lower end of the λ range for turbines used in the field. This set of experiments uses a specific hub velocity of approximately 4.5 m/s. It is in the operating range of standard turbines and provides a detailed comparison to wind farm experiments completed at the same velocity. The derated tip-speed ratio for the model turbine in the undisturbed boundary layer is $\lambda \approx 4.5$, while typical values for utility-scale wind turbines range between $\lambda \approx 3.5$ and 10.

The model turbines were operated in two different states: (i) rated state; (ii) derated state. The rated state means that a voltage was applied from a DC power supply or function generator to the DC generator on the model turbine applying a torque opposing the aerodynamic torque and allowed the control of the tip-speed ratio. More details are provided in Section III.B. In the derated state, the turbine was allowed to operate under no load and produce electricity through the DC generator, which was then recorded for use in diagnostics. The turbine voltage is produced by the DC generator with a constant electrical load and mechanical torque. For more details on turbine voltage production and analysis verification the reader is directed to Howard et. al.[30]

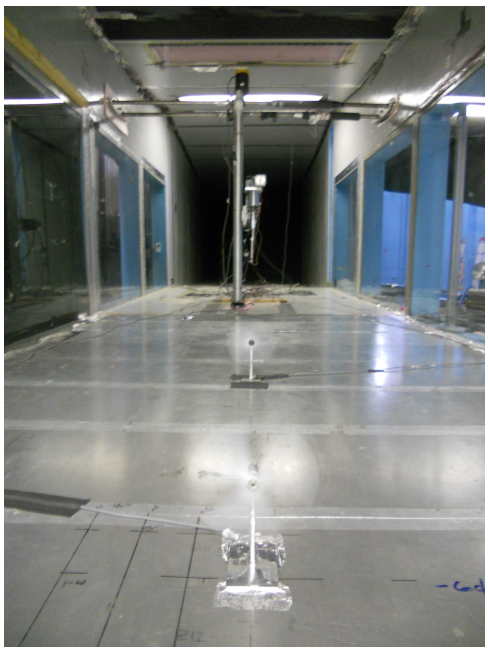

Figure 3. Two turbine setup in the SAFL wind tunnel (left) and the 2.5 MW Clipper turbine at UMore Park (right)

B. Two-Turbine Setup

Each experiment uses two model turbines placed in the wind tunnel with spacings of three to five diameters. A voltage can be applied to the generator, as described above to vary the rotor angular velocity, which in turn adjusts the performance of the turbine, as mentioned in Section II. For example, at higher generator torques, the turbine is extracting more power from the wind resulting in a lower rotor angular velocity and lower power production at the downwind turbine. The performance of the first turbine impacts the operation of the downwind turbine. Several experiments were run to examine the response of the downwind turbine based on the inputs to the upwind turbine. Square waves with varying frequencies were applied to the upwind turbine and the voltage response of the downwind turbine was recorded. A summary of the experiments can be seen in Table 1.

Model Turbine Experiments	
Turbine Spacing	**Frequencies**
3D	0.02, 0.04, 0.05, 0.067, 0.1, 0.143, 0.2, 0.5, 1.0, 2.0, 5.0, 10.0 Hz
5D	0.02, 0.04, 0.05*, 0.067, 0.1, 0.143, 0.2, 0.5, 1.0, 2.0, 5.0, 10.0 Hz

Table 1. Summary of two turbine experiments. The (*) indicates that PIV was also taken during this experiment.

As noted above, each experiment is run at a wind speed of 4.5 m/s. The frequencies in these experiments were chosen to inspect the ability of the model turbines to respond. At higher frequencies, the turbine response was limited due to the internal electrical resistance, and primarily, the rotational inertial of the rotor. In addition, the frequencies tested can be translated to relevant wind gust events for utility scale turbines. The model turbine rotor speed was measured using a tachometer and was observed to be approximately 2400 RPM, or 40 Hz. The Clipper turbine has a rotational speed of around 0.2 Hz while operating in the same region as the model turbine. As a result, the frequencies in Table 1 can be related to the Clipper turbine by scaling the perturbation frequency with a ratio of Clipper angular velocity by the model turbine angular velocity. The frequencies listed in Table 1 would translate to frequencies between 0.0001 Hz and 0.05 Hz for

the Clipper turbine. Qualitatively, these time scales correspond to winds generated during thunderstorms, which can last on the order of hours, and wind gusts, which can be on the order of tens of seconds, see Figure 4.

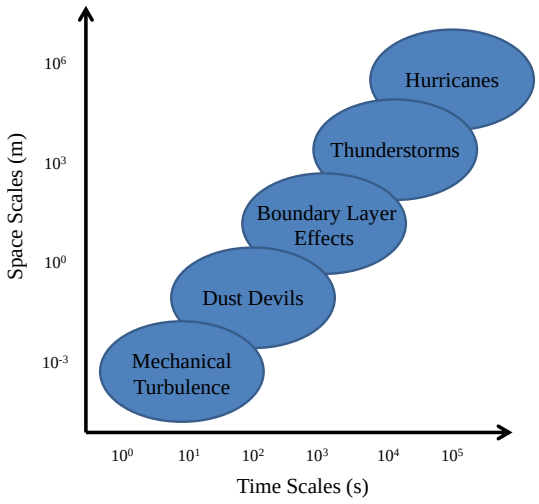

Figure 4. Time and space scales of wind events[31]

Each test was run for 100 s, limited by the maximum number of samples for the data acquisition system when sampling at 10000 Hz. Voltage measurements were taken from both turbines and PIV was used to capture the physical characteristics in the wake created by the upwind and downwind turbines. Both data types provide some insight into how the wake responds to the varying input of the upwind turbine. Specifically, PIV was used to look at wake meandering as a function of the upwind turbine input. Wake meandering is defined by the non-uniform oscillation downwind of the wake, which is typically forced by large-scale turbulent motions. Wake meandering is an important aspect to consider when performing wind farm control as it can cause significant structural loading on the turbine. It can also enhance wake recovery, which increases the amount of wind available to downwind turbines.[32]

IV. Results

In this section, PIV results are analyzed to investigate wake meandering and the changes induced by the varying inputs. In addition, the results presented look at the voltage response of the downwind turbine due to the varying input of the upwind turbine.

A. Wake Meandering

PIV was used to examine the effects of varying inputs on the wake meandering behind the upwind turbine. PIV uses a pulsating laser sheet synchronized with high resolution cameras to capture instantaneous movement of seeding particles in the wake. Olive oil droplets on the order of 5 to 10 microns in diameter are injected into the wind tunnel and tracked by taking snapshots in time and comparing the locations of the particles. The time between snapshots is known and, therefore, the velocity vectors of the particles can be computed. Figure 5 shows details of the two instantaneous velocity fields on a horizontal plane taken at hub height behind a turbine.

In the left plots, the minimum velocity is tracked and then low pass filtered to produce the white curve of Figure 5. Filtering the data gives a smooth curve in which a rough estimate of the wake meandering frequency can be determined. The right plot shows the upwind turbine operating in a derated state. The left plot shows the upwind turbine operating in a rated state and it forms a more distinct shear layer, shown by the definitive line between freestream velocity and the wake. In addition, the estimated average wake meandering frequency when the upwind turbine was in a derated state was around 33 Hz, while for a rated state, the averaged wake meandering frequency increased to 38 Hz. It is proposed that this is because the upwind turbine wake in a rated state has a larger velocity deficit, producing the strengthened shear layer

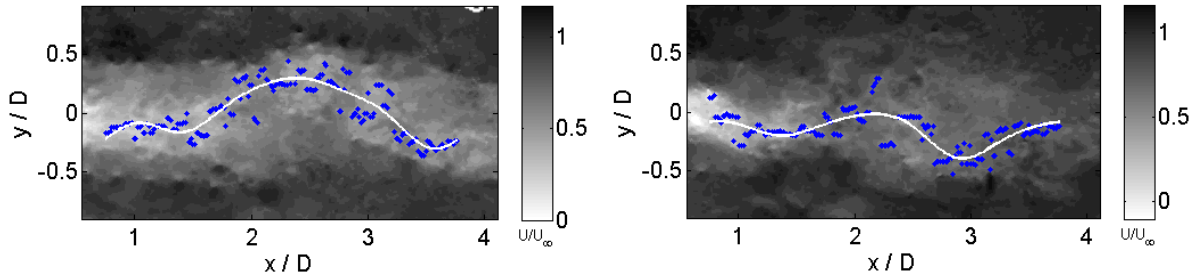

Figure 5. Instantaneous wake meandering captured by PIV. The left plot shows the turbine operating in a rated state and the right plot shows the turbine operating in a derated state.

and allowing the wake to meander more as it makes its way downwind at a slower velocity. This could have an overall effect on the turbine loads. Understanding the relationship between wake meandering and the actions of the upwind turbine may lead to better wind farm control designs that have the potential help to mitigate loads and increase the lifetime of the turbines.

B. Voltage Test Results

In addition to PIV, voltage tests were conducted to investigate the effects between a varying input and the response of the downwind turbine. Specifically, Figure 6 displays a few selected inputs to the upwind turbine and the response of the second turbine when placed downwind at 3D and 5D. The left column shows the upwind turbine input voltage signal. The middle and right columns show the downwind turbine output voltage response. The results shown are ensemble averages over the total number of periods contained in each 100 s experiment. Specifically, the results shown for 0.04 Hz, 0.1 Hz, and 1 Hz correspond to ensemble averages over 4, 10, and 100 periods, respectively. This is important to note because each plot corresponds to an ensemble average over a different number of periods.

There are several significant points to note from these results. First, when the signal on the upwind turbine has a high input, or enters a rated state, this means that the turbine is operating at a higher efficiency, and is extracting more energy out of the wind. In steady-state operation, this produces a larger velocity deficit in the wake and reduces the overall output of downwind turbine. Similarly, when the upwind turbine has a low input, or enters a derated state, it is extracting less energy from the wind, providing a higher wind speed for the downwind turbine. This is the reason for the 180° phase shift between the upwind turbine input signal and the downwind turbine output seen in the lower frequencies, most notably at 0.04 Hz (top row of Figure 6).

As the frequency increases, the voltage production of the downwind turbine tends to more closely mimic the input signal. For example, at 1 Hz (bottom row of Figure 6), the downwind turbine voltage response is nearly in phase with the upwind input signal. The difference between the run at 0.04 Hz and at 1 Hz is twofold, (i) due to the reduced convection velocity of the wake and (ii) from the change in turbine rotor inertia. The downwind turbine does not instantaneously respond to the effects of the upwind turbine operating at a higher efficiency, but at a certain amount of time later. At 1 Hz, the upwind turbine is changing its state at nearly the same time that the downwind turbine is feeling the effects of the previous state. This results in a phase lag greater than 360^o.

Another thing to note is the changing amplitude of the downwind turbine output as the turbines are spaced farther apart and the frequency is increased. As the turbine spacing is increased, the wake has more time to recover and evolve, which dampens the effect of the input from the upwind turbine. In addition, the model turbines have a certain amount of rotational inertia that prevents them from responding to fast frequencies. For example, a utility turbine can respond to large gusts of wind, but due to its large rotational inertia, it cannot respond to the microscales of turbulence. The faster the input frequency becomes, the smaller the response will be at the downwind turbine.

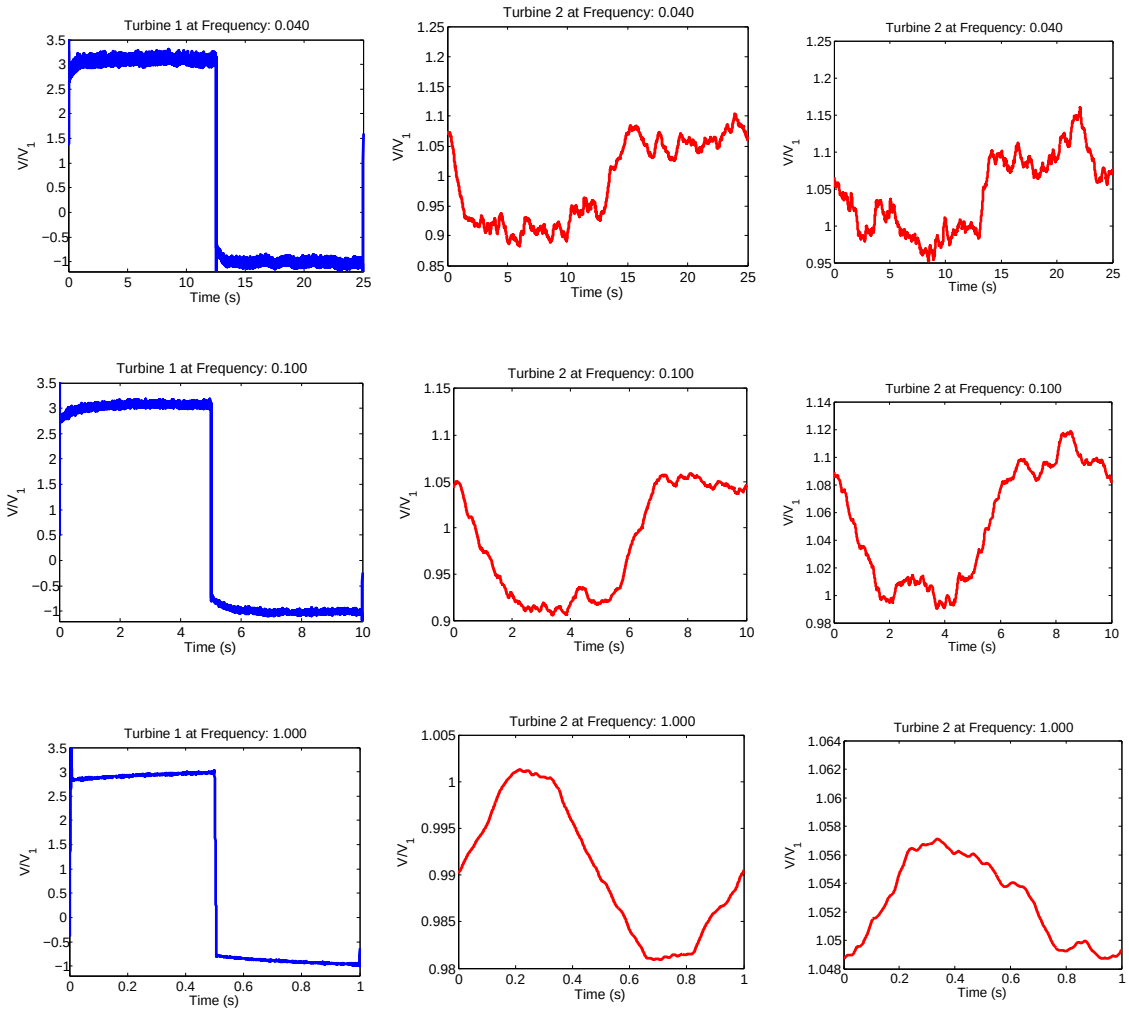

Figure 6. Voltage Results: Input square wave at upwind turbine (left), effect on downwind turbine at 3D spacing (center), effect on downwind turbine at 5D spacing (right)

V. System Identification

The objective of these experiments is to find a model suitable for dynamic feedback control (Figure 7). The input to the model developed in this paper is the generator torque, τ_{g1}, of the upwind turbine which is a function of the input voltage. The output is the voltage generated by the downwind turbine. This model could be used to coordinate turbines in a wind farm to maximize power and reduce structural loads.

Frequency domain techniques were used to construct dynamic models from upwind voltage input u to downwind voltage output y. For each experiment (turbine spacing and frequency input f), the Fourier Transfrom of the domain data samples $\{u_k, y_k\}_{k=1}^{L}$ was computed. This data consists of complex numbers $\{\hat{U}(\omega_j), \hat{Y}(\omega_j)\}_{j=1}^{L}$ that depend on the frequency ω_j. The power spectrums $(\hat{U}, \hat{Y})$ contain noise, e.g. due to 60 Hz electric interference. To eliminate the effects of this noise the ratio $\hat{G}(jf) = \hat{Y}(jf)/\hat{U}(jf)$ was computed only at the excitation frequency f of the square wave input. The magnitude and phase of this complex number $\hat{G}$ computed for each experiment is shown as a function of frequency (red dots) in Figure 7. The magnitude is shown in units of decibels: $20 \log_{10} |\hat{G}|$.

The empirical magnitude and phase data is then used to construct the dynamic model using numerical tools found in the System Identification Toolbox in MATLAB. Specifically, the function `tfest` was used to fit the data with a second-order transfer function of the form:

$$\hat{G}(s) = \frac{1}{s^2 + as + b} e^{-s\tau_d} \tag{6}$$

where a, b, and τ_d are tunable model parameters. The constant τ_d represents a time delay that is required to obtain an accurate transfer function fit. An estimate of the time delay can be computed using Taylor's Hypothesis of frozen turbulence. This hypothesis assumes that the turbulence is unchanged as it is advected downwind, i.e. wake transport from upwind to downwind. A consequence of this hypothesis is that the wake advection is only a function of the mean wind speed. For example, in the 3D case, the turbines are spaced 38.4 cm and the mean velocity is 4.5 m/s. As a result, the time delay is approximately $\tau_d = 0.09$ s. This is a conservative estimate as the wake will be moving downwind at a reduced velocity, not the mean velocity, due to the presence of the upwind turbine. The remaining parameters a and b are obtained using `tfest` to obtain the best fit. The transfer function fits obtained from the 3D and 5D experiments are given by:

$$\hat{G}_{3D}(s) = \frac{-0.1057}{s^2 + 2.98s + 3.203} e^{-0.09s} \tag{7}$$

$$\hat{G}_{5D}(s) = \frac{-0.07078}{s^2 + 2.71s + 3.195} e^{-0.14s} \tag{8}$$

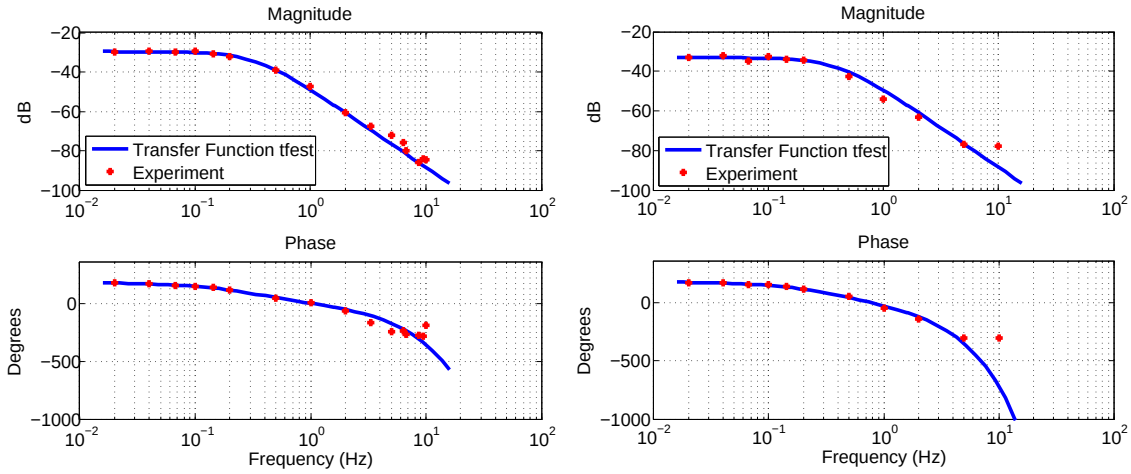

Figure 7. Frequency response of two-turbine array at 3D (left) and 5D (right) spacing

For both turbine spacings, the two-turbine array can be modeled with a second-order transfer function. The phase in Figure 7 contains the rotational dynamics of both the upwind and downwind turbine as well as information on the mean wake velocity. If rotational dynamics are ignored, the phase information can be used to determine the approximate convection velocity in the wake. The amount of phase between the input/output response reflects how long the signal took to propagate through the flow field to the downstream turbine. By analyzing the dynamic model in this way, we can get a sense of how the wake is evolving in time based on the input-output response of the two turbine array.

VI. Conclusion

A dynamic model was developed from experimental data for a two-turbine array in a wind tunnel using system identification techniques. Voltage tests were primarily used to characterize the frequency response of the system. In addition, PIV was used to identify wake meandering characteristics based on varying inputs at the upwind turbine. Both the voltage and PIV results provide insight into the wind farm control problem.

Future work includes conducting more experiments and developing control strategies around the dynamic model presented in this paper. Applying some modifications to the model turbines used in these experiments, we hope to perform wind farm control in the wind tunnel.

Acknowledgments

This work was supported by the National Science Foundation under Grant No. NSF-CMMI-1254129 entitled CAREER: Probabilistic Tools for High Reliability Monitoring and Control of Wind Farms. Any opinions, findings, and conclusions or recommendations expressed in this material are those of the authors and do not necessarily reflect the views of the NSF. In addition, the authors acknowledge the support from the Institute on the Environment, University of Minnesota (Initiative for Renewable Energy and the Environment).

References

[1]Wiser, R., "Renewable Portfolio Standards in the United States - A Status Report with Data Through 2007," LBNL-154E, Lawrence Berkeley National Laboratory, 2008.

[2]Bitar, E. and Seiler, P., "Coordinated control of a wind turbine array for power maximization," *American Control Conference*, 2013, pp. 2898–2904.

[3]Gebraad, P. M. O., van Dam, F. C., and van Wingerden, J. W., "A model-free distributed approach for wind plant control," *American Control Conference*, 2013, pp. 628–633.

[4]Johnson, K. E. and Fritsch, G., "Assessment of Extremum Seeking Control for Wind Farm Energy Production," *Wind Engineering*, Vol. 36, No. 6, 2012, pp. 701–716.

[5]Johnson, K. E. and Thomas, N., "Wind farm control: Addressing the aerodynamic interaction among wind turbines," *American Control Conference*, 2009, pp. 2104–2109.

[6]Marden, J. R., Ruben, S., and Pao, L., "A model-free approach to wind farm control using game theoretic methods," *IEEE Transactions on Control Systems Technology*, 2013, pp. 1207–1214.

[7]Schepers, J. and Van der Pijl, S., "Improved modelling of wake aerodynamics and assessment of new farm control strategies," *Journal of Physics: Conference Series*, Vol. 75 012039, 2007.

[8]Machielse, L., Barth, S., Bot, E., Hendriks, H., and Schepers, G., "Evaluation of Heat and Flux Farm Control - Final Report," ECN-E–07-105, Energy Research Centre of the Netherlands (ECN), 2007.

[9]Jensen, N. O., "A note on wind generator interaction," Tech. Rep. Risø-M-2411, Risø, 1983.

[10]Ainslie, J. F., "Calculating the flowfield in the wake of wind turbines," *Journal of Wind Engineering and Industrial Aerodynamics*, Vol. 27, No. 1, 1988, pp. 213–224.

[11]Larsen, G. C., Madsen Aagaard, H., Bingöl, F., Mann, J., Ott, S., Sørensen, J. N., Okulov, V., Troldborg, N., Nielsen, N. M., Thomsen, K., et al., *Dynamic wake meandering modeling*, Risø National Laboratory, 2007.

[12]Sørensen, J. N. and Myken, A., "Unsteady actuator disc model for horizontal axis wind turbines," *Journal of Wind Engineering and Industrial Aerodynamics*, Vol. 39, No. 1, 1992, pp. 139–149.

[13]Torres, P., van Wingerden, J.-W., and Verhaegen, M., "Modeling of the flow in wind farms for total power optimization," *Int. Conference on Control and Automation (ICCA)*, 2011, pp. 963–968.

[14]Mikkelsen, R., *Actuator disc methods applied to wind turbines*, Ph.D. thesis, Technical University of Denmark, 2003.

[15]Annoni, J., Seiler, P., Johnson, K., Fleming, P., and Gebraad, P., "Evaluating Wake Models for Wind Farm Control," *American Control Conference, Portland, OR, USA*, 2014.

[16]Yang, X. and Sotiropoulos, F., "On the predictive capabilities of LES-actuator disk model in simulating turbulence past wind turbines and farms," *American Control Conference*, 2013, pp. 2878–2883.

[17]Churchfield, M. J., Lee, S., Moriarty, P. J., Martinez, L. A., Leonardi, S., Vijayakumar, G., and Brasseur, J. G., "A large-eddy simulation of wind-plant aerodynamics," *Proc. of 50th AIAA Aerospace Sciences Meeting*, 2012, pp. 9–12.

[18]Howard, K., Hu, J., Chamorro, L., and Guala, M., "An Experimental Case Study of Complex Topographic and Atmospheric Influences on Wind Turbine Performance," *AIAA*, 2013.

[19]Howard, K. and Guala, M., "Characterizing the effects of inflow on a 2.5 MW research utility turbine," *AIAA*, 2014.

[20]Adaramola, M. and Krogstad, P.-Å., "Experimental investigation of wake effects on wind turbine performance," *Renewable Energy*, Vol. 36, No. 8, 2011, pp. 2078–2086.

[21]Krogstad, P.-Å. and Adaramola, M. S., "Performance and near wake measurements of a model horizontal axis wind turbine," *Wind Energy*, Vol. 15, No. 5, 2012, pp. 743–756.

[22]Grant, I., Smith, G., Liu, A., Infield, D., and Eich, T., "Particle image velocimetry measurements of the aerodynamics of a wind turbine," *Instrumentation in Aerospace Simulation Facilities, 1991. ICIASF'91 Record., International Congress on*, IEEE, 1991, pp. 314–320.

[23]Yang, Z., Sarkar, P., and Hu, H., "An experimental investigation on the wake characteristics of a wind turbine in an atmospheric boundary layer wind," *29th AIAA Applied Aerodynamics Conference*, 2011, pp. 1–18.

[24]Bartl, J., Pierella, F., and Sætrana, L., "Wake measurements behind an array of two model wind turbines," *Energy Procedia*, Vol. 24, 2012, pp. 305–312.

[25]Schümann, H., Pierella, F., and Sætran, L., "Experimental investigation of wind turbine wakes in the wind tunnel," *Energy Procedia*, Vol. 35, 2013, pp. 285–296.

[26]Medici, D., "Experimental studies of wind turbine wakes: power optimisation and meandering," 2005.

[27]Johnson, K. E., Pao, L. Y., Balas, M. J., and Fingersh, L. J., "Control of variable-speed wind turbines: standard and adaptive techniques for maximizing energy capture," *Control Systems, IEEE*, Vol. 26, No. 3, 2006, pp. 70–81.

[28]Pao, L. Y. and Johnson, K. E., "Control of wind turbines," *Control Systems, IEEE*, Vol. 31, No. 2, 2011, pp. 44–62.

[29]Burton, T., Jenkins, N., Sharpe, D., and Bossanyi, E., *Wind energy handbook*, John Wiley & Sons, 2011.

[30]Howard, K., Hu, J., Chamorro, L., and Guala, M., "Characterizing the response of a wind turbine model under complex inflow conditions," *Wind Energy*, 2014.

[31]Stull, R. B., *An introduction to boundary layer meteorology*, Vol. 13, Springer, 1988.

[32]Sanderse, B., "Aerodynamics of wind turbine wakes," *Energy Research Center of the Netherlands (ECN), ECN-E–09-016, Petten, The Netherlands, Tech. Rep*, 2009.